Observation of the Spin Hall Effect of Light via Weak Measurements
Onur Hosten, *et al.*
Science **319**, 787 (2008);
DOI: 10.1126/science.1152697

when not constrained by a lattice as in our experiment. The application of fundamental geometry to quantum systems is a growing field (*32*, *33*). Quantum phase extraction using topological symmetries has general applicability to the fields of quantum dots, nanoscale devices, and molecular electronics. The necessary criterion is geometric control on the scale of the relevant wavelength, already attainable in technologies such as nanolithography, self-assembly, and molecular design. Quantum dots, suitably patterned in semiconductors or metals, should mimic the physics described here, and calculations exist as a guideline for building isospectral systems (*34*). Measurements of nanomechanical resonators, now approaching the quantum limit (*35*), will similarly be phase-obscured and can benefit from these methods.

In chemistry, a complementary quest exists for isospectral and near-isospectral molecules, which can theoretically exist for a variety of different potentials but have not been experimentally observed (*36*, *37*). Just as this work allows the STM to be used as a scanning phase meter beyond charge sensitivity, we envision that other phase-sensitive experimental probes can be obtained by similar geometric tuning of quantum materials.

References and Notes

1. T. C. Weinacht, J. Ahn, P. H. Bucksbaum, *Phys. Rev. Lett.* **80**, 5508 (1998).
2. J. Itatani *et al*., *Nature* **432**, 867 (2004).
3. A. Yacoby, M. Heiblum, D. Mahalu, H. Shtrikman, *Phys. Rev. Lett.* **74**, 4047 (1995).
4. S. Marchesini, *Rev. Sci. Instrum.* **78**, 011301 (2007).
5. H. Weyl, *Nachr. Ges. Wiss. Goettingen* **1911**, 110 (1911).
6. H. P. McKean, I. M. Singer, *J. Differ. Geom.* **1**, 43 (1967).
7. M. Kac, *Am. Math. Mon.* **73**, 1 (1966).
8. J. Milnor, *Proc. Natl. Acad. Sci. U.S.A.* **51**, 542 (1964).
9. T. Sunada, *Ann. Math.* **121**, 169 (1985).
10. P. Buser, *Ann. Inst. Fourier* **36**, 167 (1986).
11. C. Gordon, D. Webb, S. Wolpert, *Inventiones Math.* **110**, 1 (1992).
12. B. Cipra, *Science* **255**, 1642 (1992).
13. See supporting material on *Science* Online.
14. S. Sridhar, A. Kudrolli, *Phys. Rev. Lett.* **72**, 2175 (1994).
15. C. Even, P. Pieranski, *Europhys. Lett.* **47**, 531 (1999).
16. E. Fradkin, J. E. Moore, *Phys. Rev. Lett.* **97**, 050404 (2006).
17. J. Kliewer *et al*., *Science* **288**, 1399 (2000).
18. P. Buser, J. Conway, P. Doyle, K. D. Semmler, *Int. Math. Res. Not.* **1994**, 391 (1994).
19. S. J. Chapman, *Am. Math. Mon.* **102**, 124 (1995).
20. M. F. Crommie, C. P. Lutz, D. M. Eigler, *Nature* **363**, 524 (1993).
21. J. A. Stroscio, D. M. Eigler, *Science* **254**, 1319 (1991).
22. M. F. Crommie, C. P. Lutz, D. M. Eigler, *Science* **262**, 218 (1993).
23. A. J. Heinrich, C. P. Lutz, J. A. Gupta, D. M. Eigler, *Science* **298**, 1381 (2002); published online 24 October 2002 (10.1126/science.1076768).
24. T. A. Driscoll, H. P. W. Gottlieb, *Phys. Rev. E* **68**, 016702 (2003).
25. A. A. Aligia, A. M. Lobos, *J. Phys. Condens. Matter* **17**, S1095 (2005).
26. E. J. Heller, M. F. Crommie, C. P. Lutz, D. M. Eigler, *Nature* **369**, 464 (1994).
27. Homophonicity is a stricter form of isospectrality. In this work, we study quantum isospectral nanostructures with Dirichlet-like boundary conditions. It has been proven that the Bilby/Hawk and Aye-aye/Beluga domains are isospectral even with Neumann boundary conditions, but homophonicity exists only within the latter pair and only for the Dirichlet case.
28. P. Bérard, *Math. Ann.* **292**, 547 (1992).
29. P. Bérard, *J. London Math. Soc.* **S2-48**, 565 (1993).
30. Tha pairs are not related by trivial transformations such as rotations, reflections, and translations.
31. T. H. Cormen, *Introduction to Algorithms* (MIT Press, Cambridge, MA, 2001).
32. L.-M. Duan, J. I. Cirac, P. Zoller, *Science* **292**, 1695 (2001).
33. M. A. Nielsen, M. R. Dowling, M. Gu, A. C. Doherty, *Science* **311**, 1133 (2006).
34. P. A. Knipp, T. L. Reinecke, *Phys. Rev. B* **54**, 1880 (1996).
35. M. D. LaHaye, O. Buu, B. Camarota, K. C. Schwab, *Science* **304**, 74 (2004).
36. W. C. Herndon, M. L. Ellzey, *Tetrahedron* **31**, 99 (1975).
37. E. Heilbronner, T. B. Jones, *J. Am. Chem. Soc.* **100**, 6506 (1978).

38. Supported by NSF grants CAREER DMR-0135122 and IMR DMR-0216913, U.S. Department of Energy grant DE-AC02-76SF00515, Office of Naval Research grant YIP/PECASE N00014-02-1-0351, Research Corporation grant RI0883, Stanford-IBM Center for Probing the Nanoscale grant NSF PHY-0425897, National Defense Science and Engineering Graduate program fellowships (C.R.M. and B.K.F.), and an Alfred P. Sloan Foundation fellowship (H.C.M.). We thank R. E. Schwartz, S.-H. Song, A. C. Manoharan, J. T. Moon, D. P. Arovas, M. Zworski, and M. R. Beasley for discussions, and R. G. Harris for expert technical assistance.

Supporting Online Material

www.sciencemag.org/cgi/content/full/319/5864/782/DC1
SOM Text
Materials and Methods
Figs. S1 to S6
Movies S1 to S3
References

9 October 2007; accepted 18 December 2007
10.1126/science.1151490

Observation of the Spin Hall Effect of Light via Weak Measurements

Onur Hosten* and Paul Kwiat

We have detected a spin-dependent displacement perpendicular to the refractive index gradient for photons passing through an air-glass interface. The effect is the photonic version of the spin Hall effect in electronic systems, indicating the universality of the effect for particles of different nature. Treating the effect as a weak measurement of the spin projection of the photons, we used a preselection and postselection technique on the spin state to enhance the original displacement by nearly four orders of magnitude, attaining sensitivity to displacements of ~1 angstrom. The spin Hall effect can be used for manipulating photonic angular momentum states, and the measurement technique holds promise for precision metrology.

Hall effects, in general, are transport phenomena, in which an applied field on the particles results in a motion perpendicular to the field. Unlike the traditional Hall effect and its quantum versions, in which the effect depends on the electrical charge, the spin Hall effect is driven by the spin state of the particles. It was recently suggested (*1*, *2*) and observed (*3*) that, even in the absence of any scattering impurities, when an electric field is applied to a semiconductor, a dissipationless spin-dependent current perpendicular to the field can be generated. A photonic version of the effect—the spin Hall effect of light (SHEL)—was recently proposed (*4*) in which the spin-1 photons play the role of the spin-1/2 charges, and a refractive index gradient plays the role of the electric potential gradient.

We use an air-glass interface to demonstrate the SHEL, in which the transmitted beam of light splits by a fraction of the wavelength, upon refraction at the interface, into its two spin components (Fig. 1A): the component parallel ($s = +1$, right-circularly polarized) and antiparallel ($s = -1$, left-circularly polarized) to the central wave vector. This effect is different from (i) the previously measured (*5*) longitudinal Goos-Hänchen (*6*) and transverse Imbert-Fedorov (*7*, *8*) shifts in total internal reflection, which are described in terms of evanescent wave penetration, and (ii) the recently reported "optical spin Hall effect," which deals with optically generated spin currents of exciton-polaritons in a semiconductor microcavity (*9*). The splitting in the SHEL, implied by angular momentum conservation, takes place as a result of an effective spin-orbit interaction. The same interaction also leads to other effects such as the optical Magnus effect (*10*, *11*), the fine-splitting of the energy levels of an optical resonator (*12*) [in which the interaction resembles the spin-orbit (Russell-Saunders) coupling of electrons in atoms], and the deviation of photons from the simple geodesic paths of general relativity (*13*).

The exact amount of the transverse displacements due to the SHEL at an air-glass interface has been the subject of a recent debate (*4*, *14*–*16*). Our theory and experimental results support the predictions of Bliokh and Bliokh (*15*, *16*); although the calculations of other researchers (*4*, *11*, *14*) are not incorrect, they contain rather unfavorable initial conditions [see supporting online material (SOM)]. One can obtain close estimates of the magnitude of the displacements using solely the conservation of the z component of the total (spin plus orbital) angular mo-

Department of Physics, University of Illinois at Urbana-Champaign, Urbana, IL 61801, USA.

*To whom correspondence should be addressed. E-mail: hosten@uiuc.edu

mentum resulting from the rotational symmetry. However, only in certain circumstances will the result be exact (*16*). [For a general review of light's angular momentum, see (*17*).]

We can describe the SHEL as a consequence of a geometric phase (Berry's phase) (*18*), which corresponds to the spin-orbit interaction. It is already known that photons, when guided by an optical fiber with torsion, acquire a geometric phase whose sign is determined by the spin state (*19*, *20*). When a photonic wave packet changes direction because of a spatial variation in the refractive index, the plane-wave components with different wave vectors experience different geometric phases, affecting the spatial profile and resulting in the SHEL.

For a paraxial beam, the transverse beam state (for the relevant direction y and its associated wave vector k_y) at the air side of the interface (Fig. 1A), including the spin state $|s\rangle$, can be written as $|\Psi_a\rangle = \int dy\Psi(y)|y\rangle|s\rangle = \int dk_y\Phi(k_y)|k_y\rangle|s\rangle$, with $\Phi(k_y)$ being the Fourier transform of $\Psi(y)$. At the glass side of the interface, under the action of the geometric phases, the state becomes $|\Psi_g\rangle = \int dk_y\Phi(k_y)\exp(-ik_y\hat{\sigma}_3\delta)|k_y|s\rangle = \int dy\Psi(y - s\delta)|y\rangle|s\rangle$, with $\hat{\sigma}_3|s\rangle = s|s\rangle$, indicating $+\delta$ and $-\delta$ shifts for the wave packets of the parallel and antiparallel spin states. Here, the term $\exp(-ik_y\hat{\sigma}_3\delta)$ represents a coupling between the spin and the transverse momentum of the photons.

The origin of this "spin-orbit" interaction term lies in the transverse nature of the photon polarization: The polarizations associated with the plane-wave components experience different rotations in order to satisfy the transversality after refraction. This is depicted pictorially in Fig. 1B with incoming horizontal polarization ($|H\rangle$) (along x_I). In the spin basis, this state corresponds to $|H\rangle = \frac{1}{\sqrt{2}}(|+\rangle + |-\rangle)$. In the lowest-order approximation, the change in the state after refraction is $|k_y\rangle|H\rangle \rightarrow |k_y\rangle(|H\rangle + k_y\delta|V\rangle) = |k_y\rangle|\varphi\rangle$, with $\varphi = k_y\delta << 1$ and $|V\rangle$ being vertical polarization. In the spin basis, $|\varphi\rangle = \frac{1}{\sqrt{2}}(\exp(-ik_y\delta)|+\rangle + \exp(ik_y\delta)|-\rangle)$, indicating the coupling $\exp(-ik_y\hat{\sigma}_3\delta)$.

As a result of the polarization-dependent Fresnel reflections at the interface, the opposite displacements of the two spin components actually depend on the input polarization state (see SOM for details). For $|H\rangle$ and $|V\rangle$ input polarizations, the displacements δ^H and δ^V are given by (Fig. 1C)

$$\delta^H_{|\pm\rangle} = \pm\frac{\lambda}{2\pi}\frac{\cos(\theta_T) - (t_s/t_p)\cos(\theta_I)}{\sin(\theta_I)},$$

$$\delta^V_{|\pm\rangle} = \pm\frac{\lambda}{2\pi}\frac{\cos(\theta_T) - (t_p/t_s)\cos(\theta_I)}{\sin(\theta_I)} \quad (1)$$

Here, θ_I and θ_T are, respectively, the central incident and transmitted angles related by Snell's law; t_s and t_p are the Fresnel transmission coefficients at θ_I; and λ is the wavelength of the light in the incident medium. In a continuously varying refractive index, the input polarization dependence disappears, and the motion can be formulated in terms of a particle moving in a vector potential in momentum space (*4*, *14*, *21*, *22*), along the same lines as with electronic systems (*23*, *24*).

For optical wavelengths, precise characterization of the displacements requires measurement sensitivities at the angstrom level. To achieve this sensitivity, we use a signal enhancement technique known from quantum weak measurements (*25*). In a quantum measurement, a property (observable $\hat{\mathbf{A}}$) of a system is first coupled to a separate degree of freedom (the "meter"), and then the information about the state of the observable is read out from the meter. At the single-photon level, the SHEL is actually equivalent to a quantum measurement of the spin projection along the central propagation direction (observable $\hat{\sigma}_3$, with eigenstates $|+\rangle$ and $|-\rangle$), with the transverse spatial distribution serving as the meter [similar to a Stern-Gerlach spin-projection measurement (*26*)]. However, the displacements generated by the SHEL here are much smaller than the width of the transverse distribution, resulting in a weak measurement: The meter states associated with different spin eigenstates overlap to a large extent. Therefore, the meter carries very little information about the state of the observable, leaving the initial state almost undisturbed. Although our experiment is at a classical level with a large number of photons in a quantum-mechanical coherent state, the results remain the same, with each photon behaving independently. Furthermore, in the paraxial regime, the dynamics of the transverse distribution are given by the Schrödinger equation with time replaced by path length, making the analysis identical to nonrelativistic quantum mechanics with an impulsive measurement interaction Hamiltonian $H_I = k_y\hat{\mathbf{A}}\delta$.

With the weak measurement taking place in between, the signal enhancement technique uses an appropriate preselection and postselection of the state of the observable to achieve an enhanced displacement in the meter distribution (*25*, *27*) (Fig. 2A). Given the preselected and postselected states $|\psi_1\rangle$ and $|\psi_2\rangle$, for sufficiently weak measurement strengths, the final position of the meter is proportional to the real part of the so-called "weak value" of the measured observable $\hat{\mathbf{A}}$

$$A_w = \frac{\langle\psi_2|\hat{\mathbf{A}}|\psi_1\rangle}{\langle\psi_2|\psi_1\rangle} \quad (2)$$

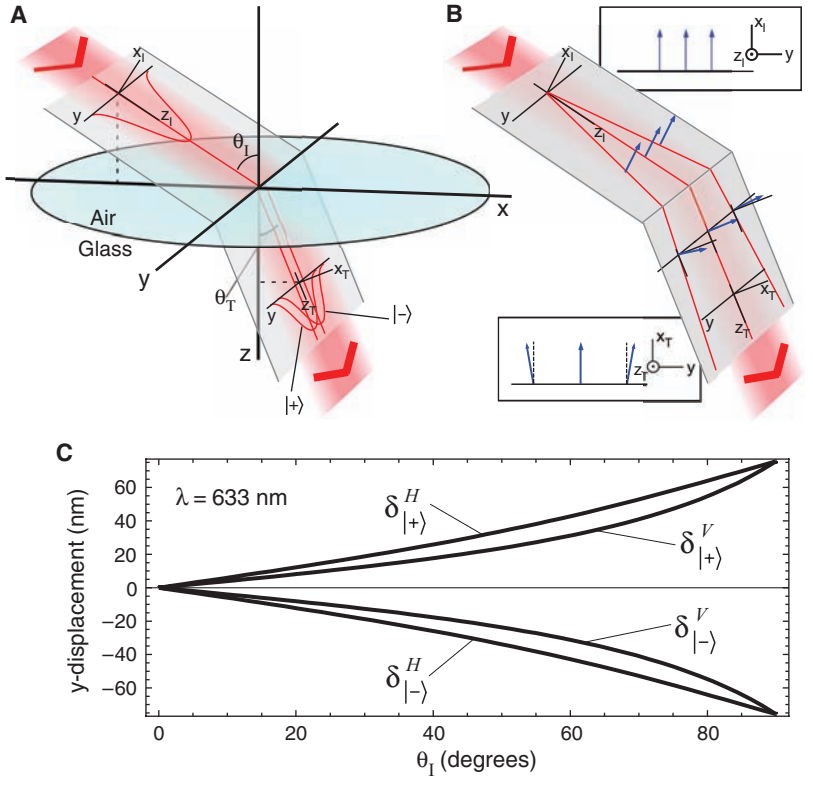

Fig. 1. The SHEL at an air-glass interface. (**A**) $|+\rangle$ and $|-\rangle$ spin components of a wave packet incident at angle θ_I experience opposite transverse displacements (not deflections) upon refraction at an angle θ_T. (**B**) Different plane-wave components acquire different polarization rotations upon refraction to satisfy transversality. The input polarization is in the x_I direction (equivalent to horizontal according to Fig. 3) for all constituent plane waves. Arrows indicate the polarization vectors associated with each plane wave before and after refraction. The insets clarify the orientation of the vectors. (**C**) Theoretical displacements of the spin components (Eq. 1) for horizontally and vertically polarized incident photons with wavelength λ = 633 nm.

which increases as the postselected state approaches being orthogonal to the preselected one. This effect was previously demonstrated (*28*) with real weak values, where a birefringent displacement of photons was enhanced by a factor of 20. The imaginary part of a weak value corresponds to a displacement in the momentum-space distribution of the meter, which with free evolution leads to the possibility of even larger enhancements. Furthermore, the order does not matter: The free evolution can take place first, followed by the weak measurement, but the final displacement will be identical (Fig. 2B). We describe the final displacement of the meter as the "modified weak value," $A_w^{mod} = F|A_w|$, where the factor F depends on the initial state of the meter and the amount of its free evolution before detection (see SOM).

In our setup (Fig. 3), the SHEL takes place at the front surface of a variable angle prism (VAP) for various incidence angles θ_I, with the back surface adjusted to be at normal incidence to avoid secondary Hall shifts (because there is obviously no Hall shift at normal incidence). The VAP is constructed by attaching two BK7 round wedge prisms together with the surface tension of a thin layer of index-matching fluid and is mounted loosely to avoid any stress-induced birefringence. The prisms can rotate with respect to each other, and the entire assembly can rotate around three orthogonal axes, allowing the desired surface orientations. The enhancement effect is achieved by preselecting and postselecting the polarization states of the incoming photons in states $|\psi_1\rangle$ and $|\psi_2\rangle$, by the calcite polarizers P1 and P2, respectively

$$|\psi_1\rangle = |H\rangle = \frac{1}{\sqrt{2}}(|+\rangle + |-\rangle),$$

$$|\psi_2\rangle = |V \pm \Delta\rangle = -i\exp(\mp i\Delta)|+\rangle + i\exp(\pm i\Delta)|-\rangle \quad (3)$$

With $\Delta << 1$ being a small angle, the weak value of the spin component is given by $(\hat{\sigma}_3)_w = \mp i\cot\Delta \approx \mp i/\Delta$. Lenses L1 and L2, respectively, focus and collimate the transverse spatial distribution of the incoming photons. The factor F in the modified weak value is determined by the transverse spatial state of the photons after lens L2 (see SOM)

$$F = \frac{4\pi\langle y_{L2}^2\rangle}{z_{eff}\lambda} \quad (4)$$

Here, $\langle y_{L2}^2\rangle$ is the variance of the y-direction transverse distribution after lens L2, and z_{eff} = 125 ± 5 mm is the effective focal length of L2. The design of the VAP assures that the optical path length inside of the VAP remains the same for all incidence angles, so that F is always the same. We achieve a displacement at the position sensor by an amount that is $(\hat{\sigma}_3)_w^{mod} = \mp F\cot\Delta \approx \mp F/\Delta$ times (~10^4 for our system) larger than the displacement caused by the SHEL

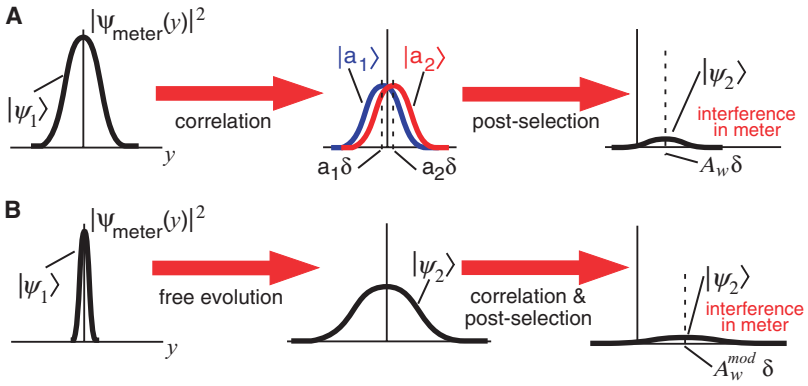

Fig. 2. A weak quantum measurement with preselection and postselection. (**A**) System starts in state $|\psi_1\rangle$. The measurement interaction weakly correlates the meter with the eigenstates of the measured observable $\hat{\mathbf{A}}$. A postselection on the system in state $|\psi_2\rangle$ gives rise to an interference in the meter, shifting it to its final position proportional to A_w (Eq. 2). (**B**) When A_w is imaginary, modifying the state of the meter by means of a free evolution (either before or after the measurement of $\hat{\mathbf{A}}$; the "before" condition is shown here) makes the final meter position proportional to A_w^{mod}, which can be much larger than A_w.

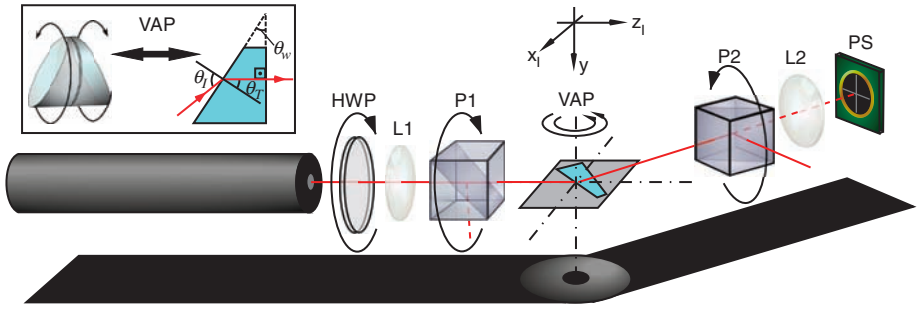

Fig. 3. Experimental setup for characterizing the SHEL. VAP (material: BK7; refractive index n = 1.515 at 633 nm); P1 and P2, Glan Laser polarizers; L1 and L2, lenses with effective focal lengths 25 and 125 mm, respectively; PS, position sensor (a split photodiode); HWP, half-wave plate (for adjusting the intensity after P1). The light source is a 10-mW linearly polarized He-Ne laser at 633 nm.

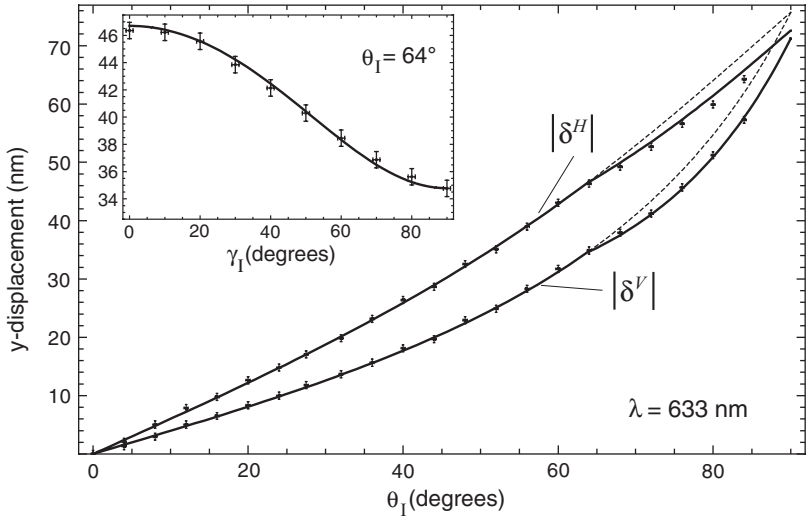

Fig. 4. Experimental results for the magnitude of the opposite shifts of the two spin components as a function of incidence angle. The data sets $|\delta^H|$ and $|\delta^V|$ are half the measured separation between the two spin components for horizontal and vertical incident polarization, respectively. Error bars represent two SDs. Dashed lines indicate the theory (Eq. 1), whereas solid lines indicate the modified theory (see text). The inset shows the results as a function of the incident polarization angle γ_I for a fixed incidence angle of 64°.

alone, and we measure this by reading out the difference between the displacements for the two postselections $|V\pm\Delta\rangle$.

In the results (Fig. 4), the dashed lines, which overlap with the solid lines up to 64°, represent the theory with the photons exiting the prism at normal incidence (Eq. 1). The solid lines also take into account the modifications (see SOM) arising from the fact that our VAP cannot satisfy the normal exiting condition beyond 64°. In order to stay in the linear response regime of both the enhancement technique and the position sensor, for incidence angles larger than 56°, the enhancement is adjusted (through the polarizer angle Δ) to be lower by a factor of 1.8: $|(\hat{\sigma}_3)_w| = 57.3 \pm 0.7$ for $\theta_I \leq 56°$, $|(\hat{\sigma}_3)_w| = 31.8 \pm 0.2$ for $\theta_I > 56°$. With the value of F determined from a single-parameter fit to be 156 ± 2, all the data points lie on the theoretical curves (Fig. 4) with a SD of 3.5 Å from the theory (excluding the last two data points of curve $|\delta^H|$, where there is a small, and as yet unexplained, discrepancy). By measuring $\langle y_{L2}^2 \rangle$, we can also experimentally determine the value of F, albeit less accurately; we find 157 ± 6, indicating the total enhancement factor to be $(\hat{\sigma}_3)_w^{mod} = (8.97 \pm 0.36) \times 10^3$ for $\theta_I \leq 56°$ and $(\hat{\sigma}_3)_w^{mod} = (4.99 \pm 0.20) \times 10^3$ for $\theta_I > 56°$. Figure 4 also shows the dependence of the displacements on the incident linear polarization (see SOM for the theory). For arbitrary incident polarization (other than $|H\rangle$ or $|V\rangle$), a kick in the y momentum is also expected; however, our measurements are not sensitive to this effect (see SOM).

The measurability of very small displacements is ultimately limited by the quantum noise of the light, because enough photons need to be collected to resolve the position of the transverse distribution (*29*). If the experiment is already quantum noise–limited, then (for a fixed number of photons entering the experimental setup) the enhancement due to preselection and postselection does not bring any gain in the measurement sensitivity: For any value of F, although the displacement is multiplied by a factor of $|(\hat{\sigma}_3)_w| \approx 1/\Delta$, only a fraction of the photons ($|\langle\psi_1|\psi_2\rangle|^2 = \sin^2 \Delta \approx \Delta^2$) makes it through the postselection, which cancels the advantage of the enhancement. Nevertheless, most experiments are limited by technical issues [e.g., in our setup, by the laser pointing stability, the intensity saturation of the position sensor, or the unwanted (~10-μm) displacements caused by rotating the polarizers]. In the experiment, we suppress all these technical issues by a factor of $(\hat{\sigma}_3)_w^{mod} \approx 10^4$ with respect to the signal and achieve a dc sensitivity/stability to displacements of ~1 Å, without the need for vibration or air-fluctuation isolation. The upper limit to the enhancement comes from the achievable extinction ratio of the polarizers and from the electronic noise in the position sensor.

The overall sensitivity of our measurements can be increased by orders of magnitude, by incorporating standard signal modulation and lock-in detection techniques, and thus holds great promise for precision metrology. In fact, in principle, Hall displacements themselves can be made arbitrarily large, separating beams associated with different spin states (*4*, *21*) [and also with different orbital angular momentum states (*22*)]. In addition, the SHEL itself may become an advantageous metrological tool (e.g., for characterizing refractive index variations measured at subwavelength distances from the region of interest, because any Hall displacement accompanying a beam deflection is larger than the displacement caused by the deflection itself at such propagation distances).

References

1. J. Sinova *et al.*, *Phys. Rev. Lett.* **92**, 126603 (2004).
2. S. Murakami, N. Nagaosa, S. C. Zhang, *Science* **301**, 1348 (2003).
3. J. Wunderlich, B. Kaestner, J. Sinova, T. Jungwirth, *Phys. Rev. Lett.* **94**, 047204 (2005).
4. M. Onoda, S. Murakami, N. Nagaosa, *Phys. Rev. Lett.* **93**, 083901 (2004).
5. F. Pillon, H. Gilles, S. Girard, *Appl. Opt.* **43**, 1863 (2004).
6. F. Goos, H. Hänchen, *Ann. Phys. (Leipzig)* **1**, 333 (1947).
7. F. I. Fedorov, *Dokl. Akad. Nauk SSSR* **105**, 465 (1955).
8. C. Imbert, *Phys. Rev. D* **5**, 787 (1972).
9. C. Leyder *et al.*, *Nat. Phys.* **3**, 628 (2007).
10. A. V. Dooghin, N. D. Kundikova, V. S. Liberman, B. Ya. Zel'dovich, *Phys. Rev. A* **45**, 8204 (1992).
11. V. S. Liberman, B. Ya. Zel'dovich, *Phys. Rev. A* **46**, 5199 (1992).
12. K. Yu. Bliokh, D. Yu. Frolov, *Opt. Commun.* **250**, 321 (2005).
13. P. Gosselin, A. Berard, H. Mohrbach, *Phys. Rev. D* **75**, 084035 (2007).
14. M. Onoda, S. Murakami, N. Nagaosa, *Phys. Rev. E Stat. Nonlin. Soft Matter Phys.* **74**, 066610 (2006).
15. K. Yu. Bliokh, Y. P. Bliokh, *Phys. Rev. Lett.* **96**, 073903 (2006).
16. K. Yu. Bliokh, Y. P. Bliokh, *Phys. Rev. E Stat. Nonlin. Soft Matter Phys.* **75**, 066609 (2007).
17. M. Padgett, J. Courtial, L. Allen, *Phys. Today* **57**, 35 (2004).
18. M. V. Berry, *Proc. R. Soc. London Ser. A* **392**, 45 (1984).
19. R. Y. Chiao, Y. S. Wu, *Phys. Rev. Lett.* **57**, 933 (1986).
20. A. Tomita, R. Y. Chiao, *Phys. Rev. Lett.* **57**, 937 (1986).
21. K. Yu. Bliokh, Y. P. Bliokh, *Phys. Lett. A* **333**, 181 (2004).
22. K. Yu. Bliokh, *Phys. Rev. Lett.* **97**, 043901 (2006).
23. M.-C. Chang, Q. Niu, *Phys. Rev. B* **53**, 7010 (1996).
24. G. Sundaram, Q. Niu, *Phys. Rev. B* **59**, 14915 (1999).
25. Y. Aharonov, L. Vaidman, *Phys. Rev. A* **41**, 11 (1990).
26. J. A. Wheeler, W. H. Zurek, Eds. *Quantum Theory and Measurement* (Princeton Univ. Press, Princeton, NJ, 1983).
27. J. Tollaksen, *J. Phys. Conf. Ser.* **70**, 012015 (2007).
28. N. W. M. Ritchie, J. G. Story, R. G. Hulet, *Phys. Rev. Lett.* **66**, 1107 (1991).
29. N. Treps *et al.*, *Science* **301**, 940 (2003).

Supporting Online Material

www.sciencemag.org/cgi/content/full/1152697/DC1
SOM Text
Fig. S1
References

7 November 2007; accepted 27 December 2007
Published online 10 January 2008;
10.1126/science.1152697
Include this information when citing this paper.

Bond-Selective Control of a Heterogeneously Catalyzed Reaction

Daniel R. Killelea,* Victoria L. Campbell, Nicholas S. Shuman,† Arthur L. Utz‡

Energy redistribution, including the many phonon-assisted and electronically assisted energy-exchange processes at a gas-metal interface, can hamper vibrationally mediated selectivity in chemical reactions. We establish that these limitations do not prevent bond-selective control of a heterogeneously catalyzed reaction. State-resolved gas-surface scattering measurements show that the ν_1 C-H stretch vibration in trideuteromethane (CHD_3) selectively activates C-H bond cleavage on a Ni(111) surface. Isotope-resolved detection reveals a CD_3:CHD_2 product ratio > 30:1, which contrasts with the 1:3 ratio for an isoenergetic ensemble of CHD_3 whose vibrations are statistically populated. Recent studies of vibrational energy redistribution in the gas and condensed phases suggest that other gas-surface reactions with similar vibrational energy flow dynamics might also be candidates for such bond-selective control.

Chemical bonds participate in a richly choreographed dance of stretches and bends during reaction, and the selective excitation of key reagent vibrations before reaction has long been viewed as a potentially powerful strategy for achieving bond-selective chemistry (*1*). Experiments on partially deuterated water (HOD) validated this approach for unimolecular (*2*) and bimolecular (*3*, *4*) reactions in the gas phase, and more recent studies have extended it to polyatomic molecules in the gas phase (*5*–*8*) and unimolecular reactions of adsorbates on surfaces (*9*–*12*). Vibrational excitation in inelastic electron tunneling spectroscopy (IETS) has promoted rotation of adsorbed acet-

Department of Chemistry and W. M. Keck Foundation Laboratory for Materials Chemistry, Tufts University, Medford, MA 02155, USA.

*Present address: James Franck Institute, University of Chicago, Chicago, IL 60637, USA.
†Present address: Department of Chemistry, University of North Carolina at Chapel Hill, Chapel Hill, NC 27599, USA.
‡To whom correspondence should be addressed. E-mail: arthur.utz@tufts.edu